Dual Additives for Stabilizing Li Deposition and SEI Formation in Anode-Free Li-Metal Batteries

Baolin Wu, Chunguang Chen*, Dmitri L. Danilov*, Zhiqiang Chen, Ming Jiang, Rüdiger-A. Eichel, and Peter H. L. Notten* [ID]

Anode-free Li-metal batteries are of significant interest to energy storage industries due to their intrinsically high energy. However, the accumulative Li dendrites and dead Li continuously consume active Li during cycling. That results in a short lifetime and low Coulombic efficiency of anode-free Li-metal batteries. Introducing effective electrolyte additives can improve the Li deposition homogeneity and solid electrolyte interphase (SEI) stability for anode-free Li-metal batteries. Herein, we reveal that introducing dual additives, composed of $LiAsF_6$ and fluoroethylene carbonate, into a low-cost commercial carbonate electrolyte will boost the cycle life and average Coulombic efficiency of NMC||Cu anode-free Li-metal batteries. The NMC||Cu anode-free Li-metal batteries with the dual additives exhibit a capacity retention of about 75% after 50 cycles, much higher than those with bare electrolytes (35%). The average Coulombic efficiency of the NMC||Cu anode-free Li-metal batteries with additives can maintain 98.3% over 100 cycles. In contrast, the average Coulombic efficiency without additives rapidly decline to 97% after only 50 cycles. In situ Raman measurements reveal that the prepared dual additives facilitate denser and smoother Li morphology during Li deposition. The dual additives significantly suppress the Li dendrite growth, enabling stable SEI formation on anode and cathode surfaces. Our results provide a broad view of developing low-cost and high-effective functional electrolytes for high-energy and long-life anode-free Li-metal batteries.

B. Wu, Dr. D. L. Danilov, Prof. R.-A. Eichel, Prof. P. H. L. Notten
Forschungszentrum Jülich (IEK-9), D-52425, Jülich Germany
E-mail: d.danilov@tue.nl
E-mail: p.h.l.notten@tue.nl
B. Wu, Prof. R.-A. Eichel
RWTH Aachen University, D-52074, Aachen Germany
Dr. C. Chen
LNM, Institute of Mechanics, Chinese Academy of Sciences, Beijing 100190, China
School of Engineering Sciences, University of Chinese Academy of Sciences, Beijing 100049, China
E-mail: chenchunguang@imech.ac.cn
Dr. D. L. Danilov, Dr. Z. Chen, Prof. P. H. L. Notten
Eindhoven University of Technology, P.O. Box 513 5600 MB, Eindhoven The Netherlands
Dr. M. Jiang
School of Electronics and Information, Institute of Carbon Neutrality and New Energy, Hangzhou Dianzi University, Hangzhou 310018, China
Prof. P. H. L. Notten
University of Technology Sydney, Broadway, Sydney NSW 2007, Australia
[ID] The ORCID identification number(s) for the author(s) of this article can be found under https://doi.org/10.1002/eem2.12642.

DOI: 10.1002/eem2.12642

1. Introduction

Lithium-ion batteries (LIBs) have become the critical component and technology limiting the driving range of electric vehicles (EVs).[1] Boosting the energy density of LIBs will certainly lengthen EVs' range. Li metal is regarded as the most attractive negative electrode for high-energy batteries due to its high theoretical specific capacity (3860 mAh g^{-1}) and low redox potential (-3.04 V vs standard hydrogen electrode).[2,3] However, Li-metal anode commonly suffers from intensive side reactions, low Coulombic efficiency (CE), and rapid capacity fading. These problematic issues originate from Li dendrite growth during Li plating/stripping and the continuous formation of solid electrolyte interphase (SEI), which consumes cyclable lithium.[4–6] Additionally, Li-metal batteries often use thick Li-metal foils at the anode side, which reduces batteries' energy density and causes safety concerns.[7]

Anode-free Li-metal batteries (AFLBs) with current-collector (Cu)||electrolyte||cathode||-current-collector cell configuration can be used to overcome the drawbacks of conventional Li-metal battery systems.[8,9] In AFLBs, the cathode offers active Li source for being plated on the Cu or other type of current-collector substrate. In this sense, no excess of Li metal is present in pristine AFLBs.[10,11] The absence of Li-metal anode leads to less weight, less volume, lower manufacturing costs, and therefore higher energy density than conventional Li-metal batteries.[12,13] The anode-free design was previously considered impractical due to the short cycle life and low CE, caused by unstable SEI formation, Li dendrites, and dead Li metal.[9] The Li source in AFLBs is only provided by the cathode material. Therefore, the formation of SEI and dead Li metal rapidly consume cyclable Li-ions, drastically decreasing battery capacity.[8] The CE of Li deposition must be considered while developing practical AFLBs to achieve high energy density and recyclability.

Electrolyte engineering effectively improves the CE by manipulating the Li deposition growth and the SEI composition.[14,15] In fact, engineering electrolyte is an elaborate combination of several methods, including altering organic solvents and salt chemistry, adding additives, and manipulating concentrations of all components. Introducing a functional additive is the most promising among these electrolyte engineering methods. This method can effectively control lithium metal's

plating/exfoliation behavior and modify the SEI layer's chemistry. Additives are applied in trace doses (usually <5%), making balancing the performance and cost easier.[16,17] Electrolyte additives can be categorized into two groups: Inorganic additives such as KI,[18] AlCl$_3$,[19] LiNO$_3$,[20] and LiBF$_4$;[21] Organic additives like 1, 3-dimethyl-2-imidazolidinone (DMI),[22] vinylene carbonate (VC),[23] and fluoroethylene carbonate (FEC).[24] The fluorine-containing electrolyte additives have superior kinetic reactivity, which facilitates the formation of more LiF components in the SEI layers to improve stability.[25] FEC is one of Li-metal batteries' most celebrated electrolyte additives. It forms a stable yet elastic LiF-rich SEI on Li metal.[26] Recently, many fluorine-containing salts have also been explored as additives for AFLBs, such as KPF$_6$,[27] LiPO$_2$F$_2$,[28] and lithium difluoro(oxalate)borate (LiD-FOB).[29] However, the majority of reported additives are really only effective in electrolytes with high salt concentrations but exhibit a minor effect on the performance of AFLIBs in low-concentrated electrolytes or currently commercial electrolytes. This may escalate the manufacturing costs of electrolytes and hinder actual commercial production. Therefore, exploring effective and low-cost additives for anode-free systems is essential for developing high-performance batteries.

In this work, a facile and effective dual additive of LiAsF$_6$ and FEC in a commercial carbonate electrolyte (1 M LiPF$_6$-EC/DEC/DMC (1:1:1 vol%)) is reported. The designed electrolyte is low-cost and effective in enhancing the electrochemical performance of the AFLBs using NMC532 as the cathode and bare Cu foil as the anode current collector. The NMC‖Cu cell possesses an excellent electrochemical performance with high-capacity retention of ~75% after 50 cycles and an average CE of ~98.3% in the presence of dual additives. In situ Raman measurements were performed to investigate the effect of the dual additives of LiAsF$_6$ and FEC on the morphology of deposited Li metal and formed SEI layers. The synergistic effect of LiAsF$_6$ and FEC contributes to smoother lithium plating. It suppresses the formation of Li dendrites and dead Li metal. Furthermore, F-rich SEI and CEI layers were observed to form on the Li anode and NMC cathode surfaces, facilitating the stability of anode-free cells.
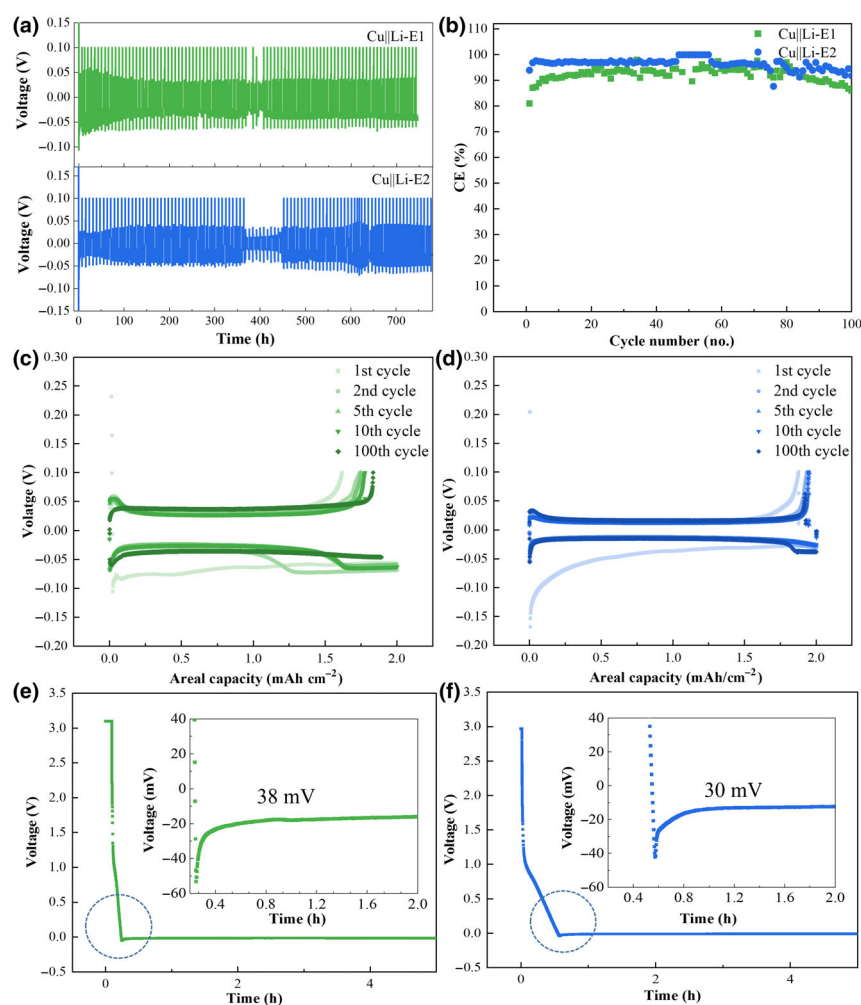

Figure 1. Electrochemical performance of Cu‖Li cells at 0.5 mA cm^{-2} current density with E1 and E2. a) Voltage profiles with E1 and E2; Polarization profile of plating/stripping process using b) E1 and c) E2; d) Coulombic efficiency curves; Voltage profiles of galvanostatic Li deposition on a copper substrate at 0.5 mA cm^{-2} with e) E1 and f) E2. E_{we} refers to the potential of the Cu current collector. A clear overpotential was observed, as circled by the dashed line. The inset shows the overpotentials of Li nucleation.

2. Results and Discussion

The Cu‖Li half-cell test was electrochemically cycled to understand polarization, capacity retention, and CE. The cyclic CE indicates the rate of Li consumption during the Li plating/stripping process and the degree of electrolyte decomposition. The electrochemical performance of Cu‖Li cell cycled at 0.5 mA cm^{-2} with the plating stripping capacity of 2 mAh cm^{-2} is shown in **Figure 1a**. The CE performance of Cu‖Li cells at 0.5 mA cm^{-2} for both E1 (LiPF$_6$ in EC/DEC/DMC 1:1:1 v/v/v ratio) and E2 (LiPF$_6$ in EC/DEC/DMC with 2% LiAsF$_6$ and FEC) electrolytes is shown in Figure 1b. The initial CE of the cells with E2 electrolytes was 90% at 0.5 mA cm^{-2}, which is higher than the initial CE of the cells with E1 electrolytes (80%). Furthermore, after a few cycles, the CE of the cells with E1 electrolytes declined, and fluctuations started. In comparison, the CE is more stable and higher in cells with E2 electrolytes. Additionally, the capacity of Cu‖Li cells with E2 electrolytes is more stable than that of cells with E1 electrolytes.

Figure 1c,d illustrates the polarization voltages of the cells with E1 and E2 electrolytes. The cells with E2 electrolyte charged and discharged at 0.5 mA cm^{-2} show a 22 and 29 mV polarization voltage for the 2nd and 10th cycles, respectively. In contrast, under the same current density, the polarization voltage was 37 and 45 mV at the 2nd and 10th cycles for the cells with E1 electrolyte. The cells with E1 exhibit more significant polarization than E2 due to the faster growth of Li dendrites.[27,30] The Li dendrites growth increases resistance due to an additional amount of SEI and dead Li-metal formation. That leads to a decline in

2 of 9

CE and capacity. Because the Li-metal anode side has a surplus of Li ions in the half Cu‖Li cell, the CE indicates the Li loss on the Cu current collector due to the decomposition of electrolytes.

To further understand the synergetic effect of the dual additives of LiAsF$_6$ and FEC on stabilizing the electrochemical performance of AFLBs, the Li nucleation overpotentials were measured. The Li nucleation overpotential probes the Li-metal nucleation and growth behavior on Cu current collectors. The voltage profiles of Li metal deposited onto bare Cu foil during the first charge process in two different electrolytes are shown in Figure 1e,f. There is a significant voltage dip at the beginning of Li-metal deposition (blue dashed circle marked), which is the Li nucleation overpotential. A flat voltage plateau follows this dip. The Li nucleation overpotential is defined as the difference between the bottom of the voltage dip and the flat part of the voltage plateau.[31] The voltage difference represents the energy necessary to overcome the heterogeneous nucleation barrier due to the large thermodynamic mismatch between Li metal and Cu. For E1, the overpotential is around 38 mV. In contrast, the overpotential for E2 is only 30 mV, indicating a lower nucleation barrier for Li metal with the dual additives of LiAsF$_6$ and FEC.[32] The dual additives facilitate the deposition of Li metal on the Cu surface. That is also beneficial to form more compact Li-metal anode.

The NMC‖Cu full AFLBs were also assembled with bare Cu as the anode current collector and LiNi$_{0.5}$Mn$_{0.3}$Co$_{0.2}$O$_2$ (NMC532) as the cathode. E1 and E2 electrolytes were used to evaluate the full-cell performance. The tests show that the capacity loss of AFLBs is only around ~14% in the first cycle, regardless of the electrolytes E1 and E2 (**Figure 2**a). This performance is much higher than the results with carbonate solvent (EC/EMC (3:7 wt %)), giving 77% capacity loss after the first charge.[33] The initial discharge capacity of NMC‖Cu cells with E2 is 3.98 mAh cm^{-2}. It is higher than the cells with E1 electrolytes

(3.85 mAh cm^{-2}). With cycling, the capacity of NMC‖Cu cells with E1 drops quickly. After 100 cycles, the discharge capacity decreased to 0.5 mAh cm^{-2}, much lower than that of cells with E2 (~2 mAh cm^{-2}). The capacity retention (Figure 2b) in E1 is below 15% after 100 cycles, comparable with earlier reported results.[30] The low CE of the cells with E1 electrolyte can be explained by the depletion of active Li metal due to the presence of free solvents. These solvents continuously react with active Li ions during the continuous plating/stripping processes. Consumption of electrolytes could be another reason because the SEI layer formed in traditional carbonate electrolytes originates from the decomposition of electrolyte solvents.[34] On the contrary, the NMC‖Cu cells with optimized electrolyte (E2) retained 75% after 50 cycles (Figure 2b) and even higher than 50% after 100 cycles. The E2-based cells exhibit a higher average CE of 98.3% after 100 cycles. From the first CV curves (Figure 2c), it was found that the current in the CV curve of E2 is higher than for E1 for the same voltage range (3–4 V). That confirms the presence of electrochemical reactions of the dual additives in this voltage range. The decomposition of the dual additives facilitates the formation of a more stable SEI layer and, therefore, improving in the stability of the anode-free cell. Figure 2d shows the influence of the current (0.1, 0.2, 0.5, 0.75, and 1 C-rate) on the discharge capacity of the anode-free cells with two different electrolytes. The initial discharge capacity of 4 mAh cm^{-2} for the NMC electrode at 0.1 C-rate is reduced to 2 mAh cm^{-2} at 1 C-rate. However, the capacity can almost be fully recovered to 3.5 mAh cm^{-2} at 0.1 C-rate after 15 cycles, indicating a better rate capability than the cells using E1 electrolytes. It is worth noting that the rate capability of the sample with E2 electrolytes is systematically better than for E1 electrolytes.

The top and cross-sectional morphological analyses of the deposited Li metal were performed. **Figure 3**a shows the morphology of the deposited Li metal on Cu with E1 electrolyte. The top and cross-section show the presence of tiny block crystal structures. After discharging, the crystal structures disappeared, and the residual Li metal became porous and non-compact (Figure 3b). After 100 cycles, many cracks are observed on the surface of the residual Li metal (Figure 3c). Such cracks suggest that the instability of the SEI is related to electrolyte composition. The thickness of the Li residues is increasing, which is attributed to the formation of dead Li metal and SEI layers, resulting in rapid capacity loss. In contrast, introducing dual additives makes the deposited Li morphology after the initial charge more uniform (Figure 3d). It can be related to the lower overpotential of Li nucleation, which is favorable for the larger size of Li nuclei. The formed Li-metal structures in E2-based cells are more compact than those with E1 (Figure 3e). More importantly, the residual Li-metal structures in E2 cells exhibited fewer cracks on the surface and were more compact after 100 cycles. In addition, the thickness of the residue for E2 is smaller than for E1 (Figure 3f), suggesting that introducing dual additives improves the stability of the formed SEI layers and suppresses the formation of dead Li metal.
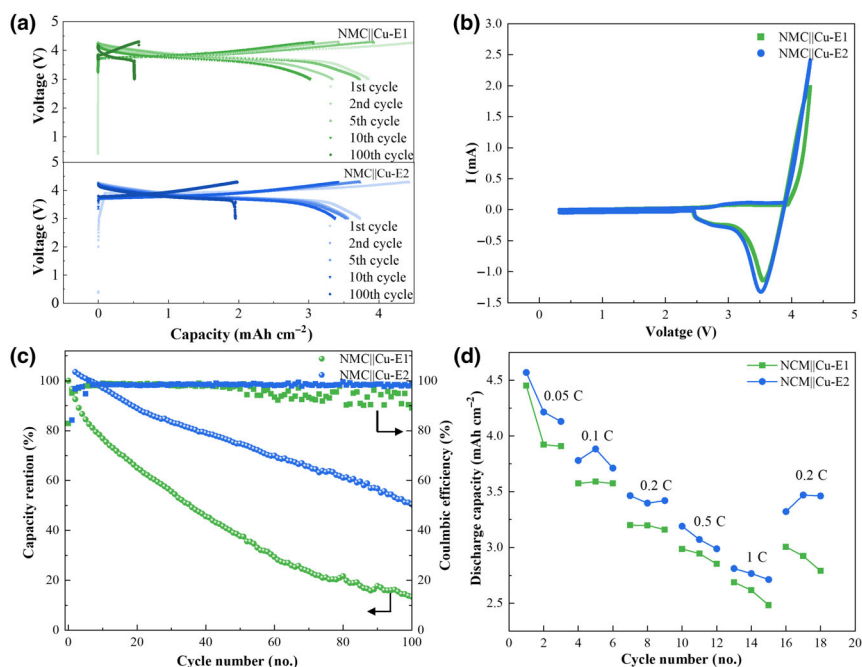

Figure 2. Electrochemical performance of NMC‖Cu cells at 0.5 mA cm^{-2} current density with E1 and E2. a) Voltage profile using E1 and E2; b) CV curves; c) Capacity retention and CE curves; d) Rate capability at various indicated C-rates.
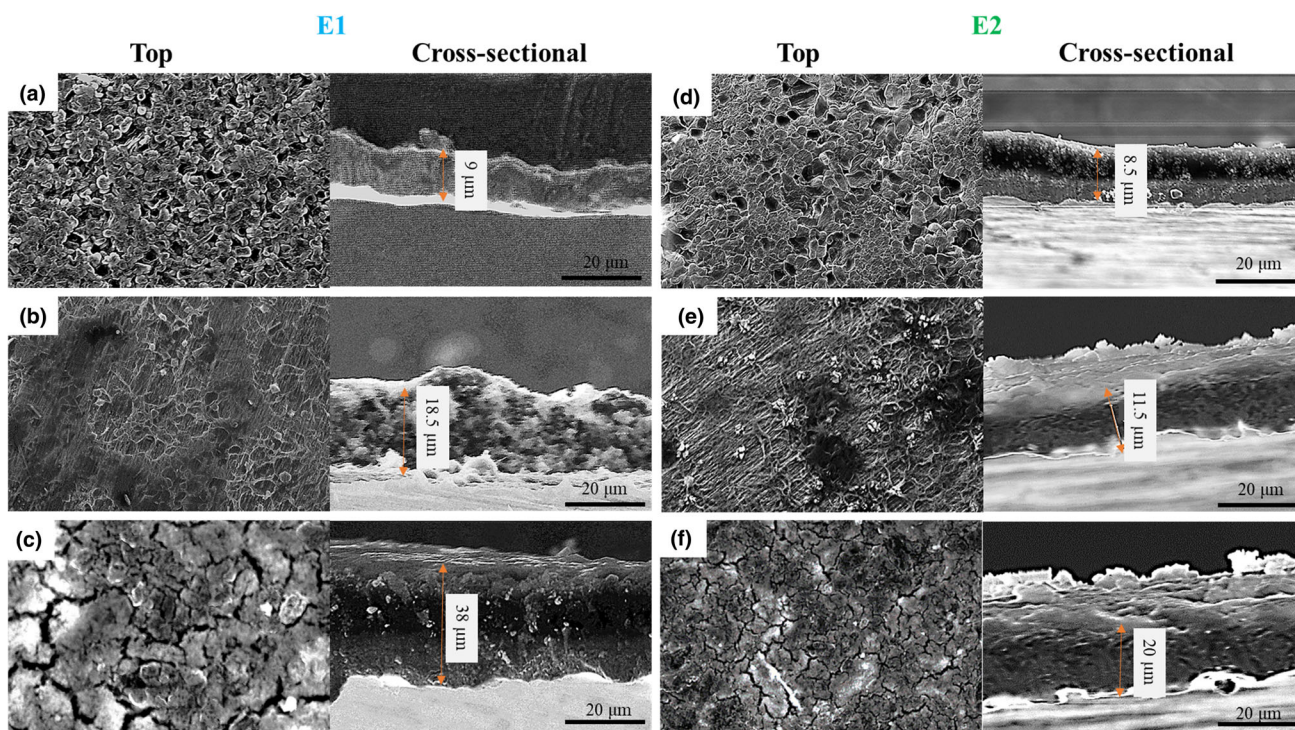
Figure 3. Top (left panel) and cross-sectional (right panel) SEM images of electrodeposited Li films on Cu substrates in different states with two electrolytes: pristine electrolyte (E1) after a) initial charged, b) first discharged, and c) 100 cycles; optimized electrolyte (E2) after d) initial charged, e) first discharged, and f) 100 cycles.
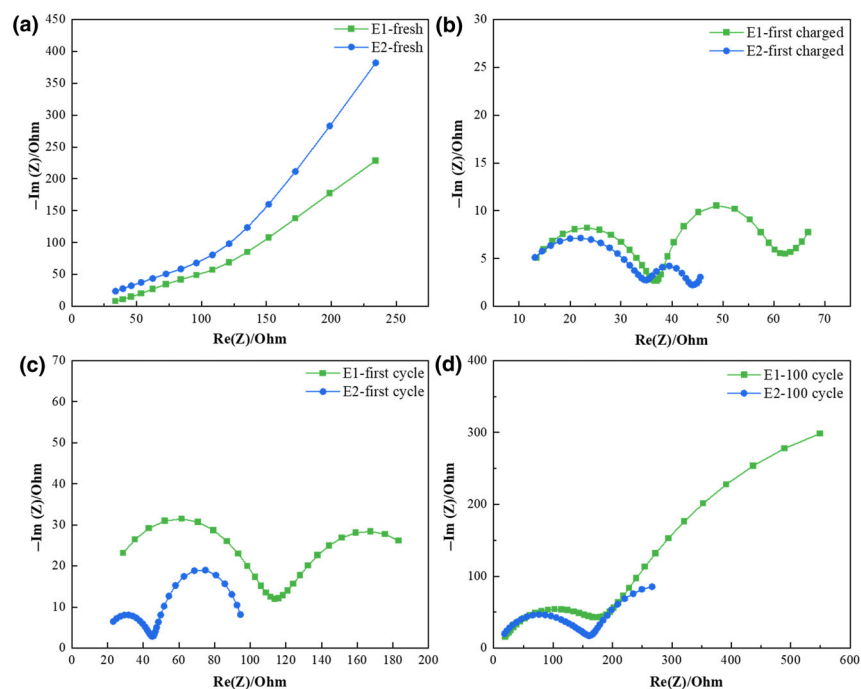

Figure 4. EIS curves of anode-free NMC‖Cu full cells that contains E1 and E2 before a) cycling, b) first charged, after c) first and d) 100th cycles.

EDX measurements on the residual Li metal after 100 cycles were performed to investigate further the effect of the dual additives on SEI formation. As shown in Figure S1, Supporting Information, C, O, F, and P elements were found in the residuals (Figure S1a, Supporting Information). These are attributed to the components of formed SEI, such as Li_2O, Li_2CO_3, LiF, $LiPO_2F_2$, and carbonate-based Li salts.[35,36] However, in comparison with the E1 electrolytes, the residues with dual additives contain arsenic, and the content of F is significantly higher (Figure S1b, Supporting Information). This observation indicates that the additives also participate in forming SEI layers during cycling. The dual additives promote the formation of Li_xAs alloy phase and LiF on the formed Li-metal surface,[37] enhancing the mechanical properties of the formed SEI layers, improving the stability.

EIS test was performed to understand the electrolyte/electrode interfacial behavior. The EIS spectra of the cells with E1 and E2 electrolytes were measured before cycling, after first charging, and after the 1st and 10th cycles. The Nyquist plots of the cells with E1 and E2

electrolytes are shown in **Figure 4**. They are with one semicircle at the high frequency, attributed to the Li$^+$ diffusion through the SEI on the surface of the electrode.[38] Figure 4a–d shows the impedance of the cells with E1 and E2 electrolytes increase continuously with cycling. The impedance increase is due to the continuous generation of SEI as well as the formation of dead Li metal. However, the cell with the E2 electrolyte has a lower impedance than that with the E1 electrolyte (Figure 4c,d). The lower impedance of E2-based cells suggests that the dual additives can effectively reduce the cell's impedance and thus

improve cell stability. Dual additives reduce the barrier of Li nucleation and guide the Li metal to grow in structures with a smoother and denser morphology. Moreover, introducing F atoms makes the SEI layer contain more LiF inorganic components. That makes the formed SEI layer more stable and contributes to reducing the cell's impedance, thus effectively improving the stability of the anode-free cell.

To further demonstrate the effect of dual additives on the Li deposition/dissolution and SEI formation, in situ Raman was performed on the NMC‖Cu cells with two different electrolytes (E1 and E2). The geometry of the in situ Raman cell is illustrated in Figure S2, Supporting Information. NMC532, with a 10 mm diameter, was used as a cathode. A glass fiber separator soaked with 50 μL E1 electrolytes was placed on top of the cathode. A 16 mm Cu mesh was placed on top of the separator. Then the glass window was pressed on the top. The cell was cycled at C/10 between 4.3 and 3.0 V. **Figure 5a** shows the morphology of the formed Li-metal structures during the first cycle. Initially, the Cu surface is shiny and smooth. After the first 30 min of plating, it was found that the deposited Li nuclei on the upper Cu surface were inhomogeneous (30-min image in Figure 5a). With Li plating proceeding, the plated Li metal show a porous structure (2 and 10 h image in Figure 5a). During the Li deposition process, the growth of inhomogeneous Li nuclei results in different Li growth rates at different locations. Then, the Li metal grows into the free space with time. The deposited Li metal exhibit a highly porous structure due to the uniform Li growth process when the formed Li-metal structures fill the free space. As the Li stripping process begins, the dissolution rate of Li metal is also inconsistent at various points. That facilitates the formation of Li dendrites and dead lithium. It can be observed that when discharged to 3 V, there is still a lot of Li metal on the copper surface as well as dendritic Li metal. That causes a significant initial capacity loss.

Figure 5. In situ Raman measurements of NMC‖Cu cells with a, b) E1 and c, d) E2 electrolytes. Microscopic images on the surface of copper current collector at different cycling states with a) E1 and c) E2 electrolytes; In situ Raman spectra for the copper current collector with b) E1 and d) E2 electrolytes during the first cycle. The potential curves (left) and pseudocolor plots (right) are shown together.

The potential curve of the first cycle and the corresponding in situ Raman spectra are shown in Figure 5b. With cycling, a peak at 1846 cm^{-1} starts to be observed, which is formed due to the symmetric stretching vibration of the triple bond of the acetylide anion in Li$_2$C$_2$.[39,40] In addition, the signal at 1070 cm^{-1} is attributed to the symmetric stretching vibration of the carbonate anion from Li$_2$CO$_3$.[41] Li$_2$CO$_3$ is an SEI product originating from the decomposition of the organic carbonates in the electrolyte.[42] During the charging process, the intensity of SEI-induced spectra (1070 and 1846 cm^{-1}) continuously grows. The intensity increase is due to the continuously formed SEI caused by the reaction between the electrolyte and newly deposited Li metal. More importantly, during the discharge process, the SEI does not disappear, even when discharged to
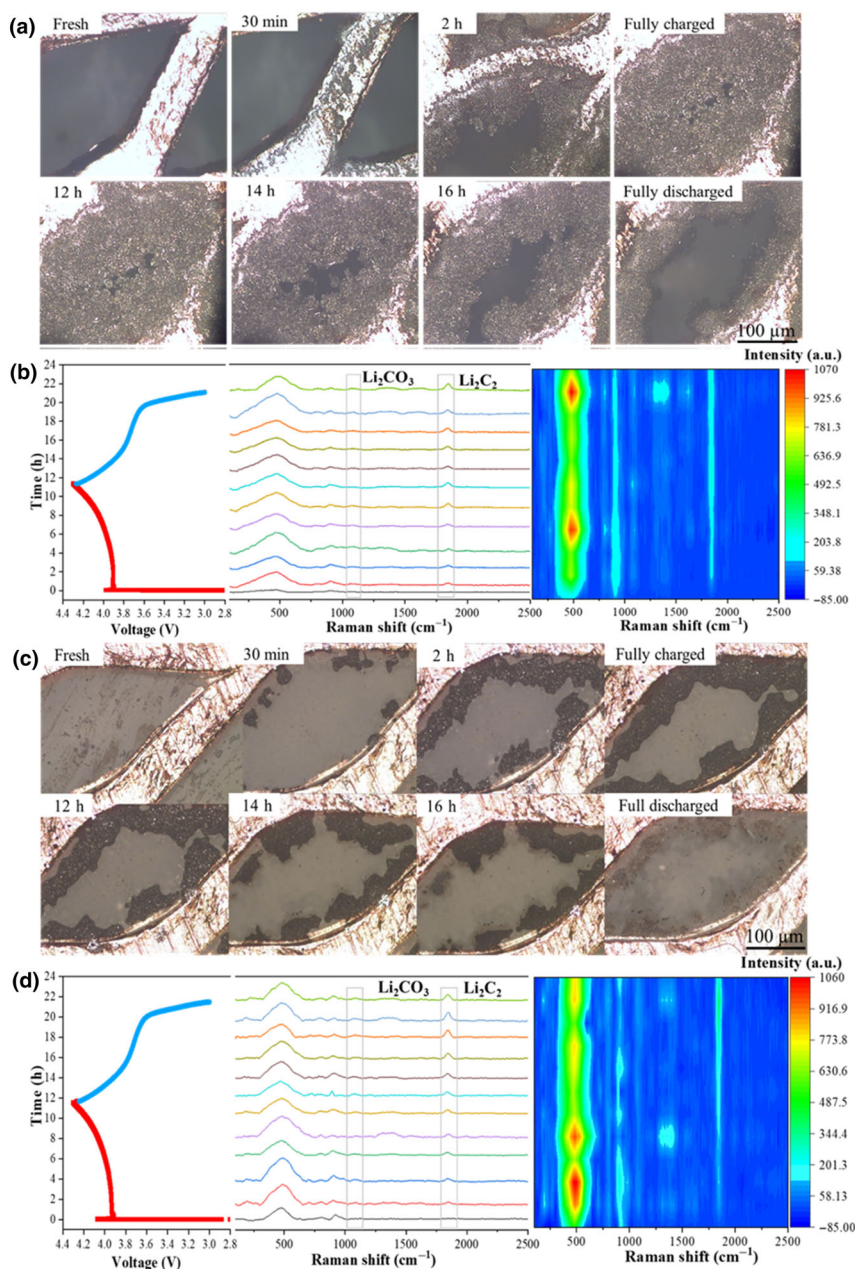
3.0 V, which is another significant cause of the large decay of initial capacity and CE. The broad signals at 470 and 910 cm^{-1} might be attributed to various origins. These signals could be from the electrolyte, for example, the ring breathing modes of EC–lithium complexes R–O and C–C stretching.[40] Another possibility could be the decomposition of the polymer-based SEI, known as organic SEI.[42]

Figure 5c shows the optical microscopy images of Li-metal plating/ stripping behavior with E2 electrolyte. In the first 30 min of Li plating (Figure 5c), the Li nuclei were preferably deposited on the bottom of the copper surface. However, when charging to 4.3 V, only a small amount of Li metal was found on the upper blank parallelogram area. That indicates more compact Li-metal structures formed on the bottom of the copper surface. In the stripping process, less rod-shaped Li metal was left. In addition, when discharged to 3 V, the earlier formed Li-metal structures on the upper Cu surface disappeared. This observation confirms that the dual additives improve Li plating and stripping reversibility. Dual additives facilitate the Li metal to form a more compact and smooth Li morphology.

Figure 5d shows in situ Raman spectra recorded during the first cycle. Similarly, SEI peaks at 1070 and 1846 cm^{-1} appeared during the charging process. The SEI peaks can still be observed after discharge to 3.0 V, indicating that the formed SEI layers are stable. That could be well-protected plated Li metal. Compared to the E1 electrolyte, E2 can increase LiF content in the SEI components, thus improving stability.

The theoretical Raman signal of LiF is at 228 cm^{-1}. However, the signal is very weak and can hardly be traced in the Raman spectra because the formed LiF layer is very thin.[43] Nevertheless, in situ Raman measurements could effectively resolve the origins of the high-capacity loss and low CE of NMC‖Cu cells by observing the formation of dead Li metal and SEI layers. LiAsF$_6$ and FEC molecules act synergistically in controlling the Li growth process and SEI formation. On the one hand, LiAsF$_6$ can be reduced to form the Li$_x$As alloy phase and LiF. The formed Li$_x$As alloy on the current collector surface facilitates the Li-deposition to generate a compact and smooth Li-metal anode.[37] In addition, the simultaneously formed LiF is an important component in SEI layers, which can improve the stability of formed SEI layers. On the other hand, the presence of FEC results in the formed SEI layers with higher concentrations of inorganic species, particularly LiF.[44] Furthermore, the organic components in the formed SEI contain less aliphatic carbon, contributing to the improved quality of SEI layers. Therefore, LiAsF$_6$ and FEC favorably work together to reduce the Li-nucleation potential barrier, promote the growth of uniform Li metal, and improve the quality of the formed SEI layers. As a result, the developed dual additive helps suppress the Li-dendrites growth and reduce the capacity loss.

In addition to the positive effects of the dual additives on the deposited Li metal, the effect on the NMC cathodes was also explored. Top and cross-sectional morphological analysis of the NMC cathodes after 100 cycles with two different electrolytes (**Figure 6**). It was shown that NMC developed many cracks after 100 cycles with E1 electrolytes (Figure 6c). In contrast, the morphology of NMC is better preserved after 100 cycles with E2 electrolytes (Figure 6e). According to the cross-sectional SEM images (Figure 6b,d,f), the NMC cycled with E2 electrolytes is more compact. In addition, the existence of the fluorine on the surface of the NMC cycled with E2 electrolytes was confirmed by EDX measurements (Figure S3, Supporting Information). This observation indicates that introducing dual additives of LiAsF$_6$ and FEC facilitates the formation of fluorine-containing composites on the surface of the NMC cathode. These composites protect the NMC and improve its cycling stability. Raman tests were performed on the NMC cathodes at different cycling states, as shown in **Figure 7**. Bands between 300 and 750 cm^{-1} correspond to metal-oxygen vibrations. Bands at 1350 and 1600 cm^{-1} refer to the Raman shifts of the carbon black conductive additive.[45,46] For the NMC cathode cycled with E1 electrolyte, the peak of at 450 and 580 cm^{-1} decreased after charge to 4.3 V. It is likely that a kind of structural (dis-)ordering transition (hexagonal phases H1, H1 + H2) happens during the charging process when the electrode is partially delithiated.[47] Subsequently, the peaks increased after full discharge. However, after 100 cycles, these peaks become weak, indicating that NMC cathode materials' structure drastically degraded. In contrast, with the E1 electrolyte, the Raman peaks of the NMC cathode are higher at 450 and
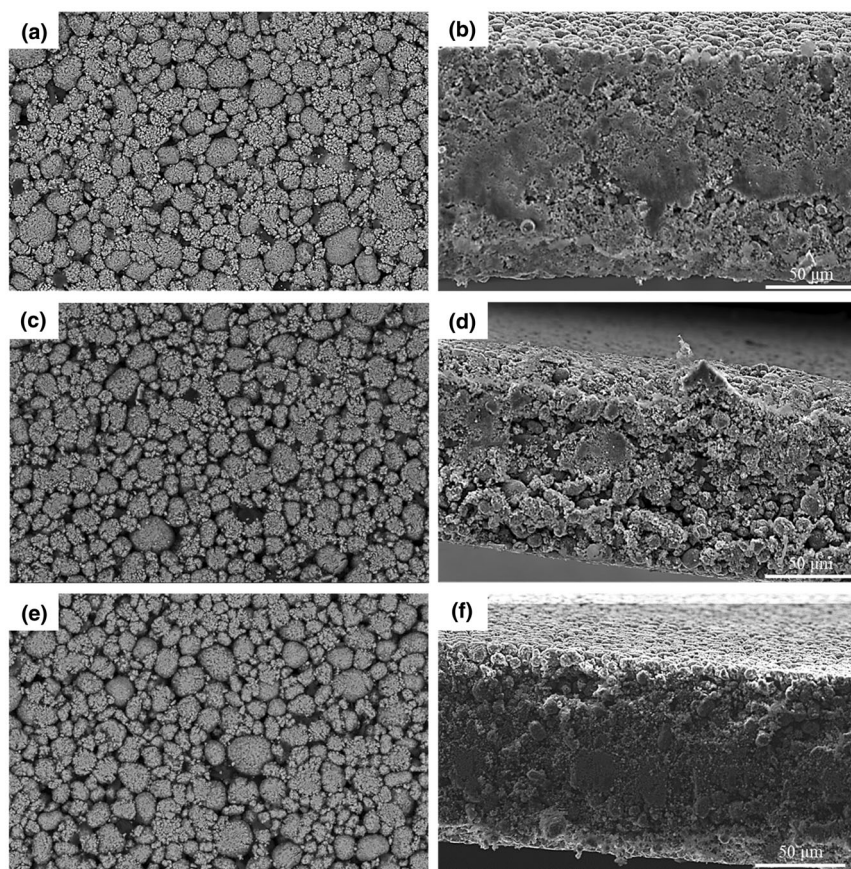

Figure 6. Top (left panel) and cross-sectional (right panel) SEM images of NMC with two electrolytes: a, b) fresh NMC cathode, c, d) after 100 cycles with pristine electrolyte and e, f) optimized electrolyte.
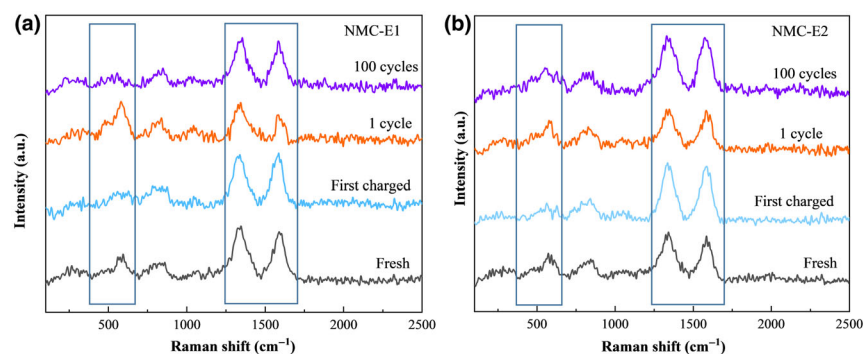
Figure 7. Raman spectra measured fresh NMC cathodes and cycled at different cycling states with a) E1 and b) E2.
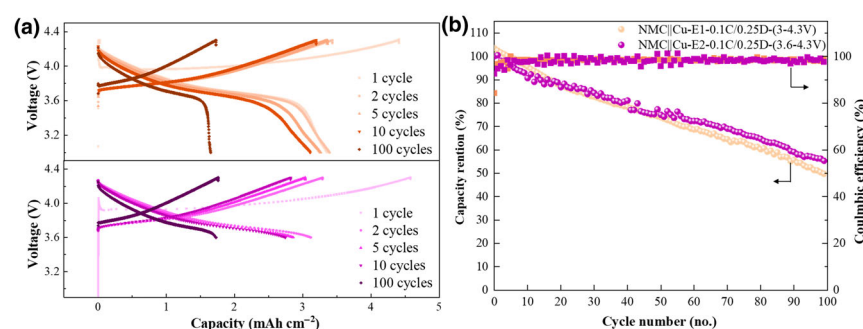

Figure 8. Electrochemical performance of NMC‖Cu cells at 0.1 C-rate charge/0.25 C-rate discharge with E2 from 3 to 4.3 V and 3.6 to 4.3 V. a) Voltage profile; b) Capacity retention and Coulombic efficiency.

3. Conclusion

The dual additives of $LiAsF_6$ and FEC in commercial carbonate electrolytes (1 M LiF_6 in EC/DMC/DEC) for anode-free lithium-ion batteries (AFLBs) are introduced to enhance the CE and capacity stability. Benefiting from the synergistic effect of the dual additives, the assembled AFLBs (NMC‖Cu geometry) could deliver a high average CE of up to 98.3% when cycled at 0.5 mA cm^{-2}. It shows a reasonably high discharge capacity retention of 75% after 50 cycles. In contrast, the pristine commercial electrolyte exhibited a lower CE of 97% and low-capacity retention of 35% after 50 cycles. In situ optical observation indicates that the introduction of dual additives induces the plating of Li metal into a more compact and conformal morphology, resulting in a reduced battery residence. Furthermore, in situ Raman measurements revealed the synergistic effect of $LiAsF_6$ and FEC additives in controlling the Li nucleation and growth to form Li columns with self-alignment in the plane. That results in more compact, uniform, and less-dendritic Li-metal anodes. It also was observed that $LiAsF_6$ and FEC could be reduced to form the Li_xAs alloy phase and LiF. That facilitates forming of solid and rigid LiF-rich interphase layers on negative and positive electrode surfaces. A deep understanding of the positive impact of additives on controlling Li growth and stable SEI layers opens up the potential for developing low cost and efficient functional electrolytes for long-life AFLBs.

580 cm^{-1} (Figure 7b), indicating that more NMC materials are active with E2 after 100 cycles. It is confirmed that the dual additives help form more stable CEI layers on the NMC surface, improving stability. Therefore, the dual additives synergistically improve the stability of both positive and negative electrodes.

The effect of various cycling conditions was further explored. It has long been established that using lower Li plating current density help improve AFLBs' lifetime by forming a compact Li-metal anode.[48] For this, an asymmetric cycling protocol was designed with 0.1 C-rate for charge and 0.25 C-rate for discharge. This cycling protocol help to minimize lithium inventory loss during Li plating and stripping.[49] As shown in **Figure 8**a, the discharge capacity decreased. However, higher capacity retention of 60% after 100 cycles was demonstrated, with a similar average CE of 98.2% (Figure 8b). Therefore, using the asymmetric cycling protocol helps to improve the stability of the battery capacity. Then, we examine the influence of the depth of discharge on the lifetime of anode-free cells. Limited depth of discharge has previously been shown to be beneficial to the lifetime of Li-metal cells.[50] Therefore, a limited cut-off voltage (3.6–4.3 V) was applied together with an asymmetric cycling protocol, which may improve the NMC cathodes' stability. The specific capacity further decreased when a limited cutoff voltage was used (Figure 8a). However, the capacity retention and CE are similar to the cutoff voltage of 3.0–4.0 V (Figure 8b).

4. Experimental Section

Electrolyte preparation: Commercially available electrolyte containing 1 M $LiPF_6$ in a mixture of ethylene carbonate (EC), diethyl carbonate (DEC), and dimethyl carbonate (DMC) (1:1:1, by volume ratio) was used as the standard electrolytes. A total of 2 wt % $LiAsF_6$ (99.9%) and 2 wt % fluoroethylene carbonate (FEC) (99%) were added and gently stirred for 24 h to prepare the optimized electrolytes. All the materials are purchased from Sigma-Aldrich.

Electrochemical measurements: Commercial 18650-type cylindrical batteries manufactured by Tianjin LiShen Battery Co., Ltd were dismantled in an argon-filled glove box, and pieces of the $LiNi_{0.5}Mn_{0.3}Co_{0.2}O_2$ (NMC532) cathodes were taken out. A bare Cu foil was cut into a 12 mm diameter disc used as the anode current collector. The active material loading is 10 mg cm^{-2} per side. A 2400-type Celgard separator (25-μm-thick) and a glass fiber separator were used as the separator. Cu‖Li half-cells and full AFLBs with NMC532 cells were investigated in Swagelok cells with 75 μL of electrolytes. The pure commercial electrolyte of $LiPF_6$ in EC/DEC/DMC 1:1:1 v/v/v ratio is denoted as E1 electrolyte. The optimized electrolyte by adding 2 wt % $LiAsF_6$ and FEC into the pristine E1 electrolyte ($LiPF_6$ in EC/DEC/DMC 1:1:1 v/v/v ratio) was named E2 electrolyte. All measurements were performed in an argon-filled glove box (<0.1 ppm oxygen and <0.1 ppm H_2O). All electrochemical tests were carried out in an MKF120 climate chamber (Binder, Germany) using a VMP3 potentiostat (Bio-

Logic, France). The amount of Li metal to be plated onto the copper surface was controlled by restricting the time. The stripping was a voltage-controlled (0.1 V) process with a constant current density of 0.5 mA cm^{-2}. Galvanostatic (dis-)charge cycling of NMC532‖Cu cells was performed in the voltage range of 3.0–4.3 V at charge–discharge rates of 0.1 C. Cyclic voltammogram (CV) tests were operated in a voltage window of 3.0–4.3 V vs Li$^+$/Li at a scan rate of 0.1 mV s^{-1}. Electrochemical impedance spectroscopy (EIS) tests were conducted with an amplitude of 10 mV in the frequency range of 10–100 kHz.

Material characterization: Scanning electron microscopy (SEM) and energy-dispersive X-ray spectroscopy (EDX) experiments were carried out using a Quanta FEG 650 (FEI) environmental scanning electron microscope operated at a voltage of 20 kV.

All Raman measurements were carried out using a Bruker Senterra Raman microscope (Bruker, Germany). Experiments were performed using a 532 nm green laser at a spectral resolution of 9–18 cm^{-1} and a confocal setup. The laser power was set to 10 mW to prevent sample damage. For the microscope, a 10 × objective was used. Five integrations were carried out with an integration time of 2 s to collect the spectra. All material surfaces were scanned by recording multiple Raman spectra pointwise on a grid with an isotropic spatial resolution of 2 μm using a 50 × magnification.

For in situ measurements, a Cu/NMC full cell was setup inside an ECC-Opto-Std (EL-CELL, Germany) cell.[47,51] NMC532 electrode with a diameter of 10 mm was used as a cathode. A 1-mm-thick glass-fiber separator (EL-CELL) soaked with ~75 μL of E1 and E2 electrolytes was placed on top of the cathode. A 16 mm Cu mesh was distributed on top of the separator and pressed onto the glass window of the cell. The cell was cycled at a constant rate of 300 μA cm^{-2} (C/10) between 4.3 and 3.0 V using a BioLogic SP-200 potentiostat (BioLogic Science Instruments, France). During cycling, Raman spectra were recorded with a time step of 2 h at the Cu mesh surface with an isotropic spatial resolution of 2 μm under 50 times magnification.

Conflict of Interest

The authors declare no conflict of interest.

Supporting Information

Supporting Information is available from the Wiley Online Library or from the author.

[1] H. Kim, G. Jeong, Y.-U. Kim, J.-H. Kim, C.-M. Park, H.-J. Sohn, *Chem. Soc. Rev.* **2013**, *42*, 9011.

[2] X.-B. Cheng, R. Zhang, C.-Z. Zhao, Q. Zhang, *Chem. Rev.* **2017**, *117*, 10403.

[3] H. H. Weldeyohannes, L. H. Abrha, Y. Nikodimos, K. N. Shitaw, T. M. Hagos, C.-J. Huang, C.-H. Wang, S.-H. Wu, W.-N. Su, B. J. Hwang, *J. Power Sources* **2021**, *506*, 230204.

[4] D. Lin, Y. Liu, Y. Cui, *Nat. Nanotechnol.* **2017**, *12*, 194.

[5] P. Albertus, S. Babinec, S. Litzelman, A. Newman, *Nat. Energy* **2018**, *3*, 16.

[6] L. Lin, L. Suo, Y. S. Hu, H. Li, X. Huang, L. Chen, *Adv. Energy Mater.* **2021**, *11*, 2003709.

[7] B. A. Jote, K. N. Shitaw, M. A. Weret, S.-C. Yang, C.-J. Huang, C.-H. Wang, Y.-T. Weng, S.-H. Wu, W.-N. Su, B. J. Hwang, *J. Power Sources* **2022**, *532*, 231303.

[8] M. Genovese, A. J. Louli, R. Weber, S. Hames, J. R. Dahn, *J. Electrochem. Soc.* **2018**, *165*, A3321.

[9] C. J. Huang, B. Thirumalraj, H. C. Tao, K. N. Shitaw, H. Sutiono, T. T. Hagos, T. T. Beyene, L. M. Kuo, C. C. Wang, S. H. Wu, W. N. Su, B. J. Hwang, *Nat. Commun.* **2021**, *12*, 1452.

[10] D. W. Kang, J. Moon, H.-Y. Choi, H.-C. Shin, B. G. Kim, *J. Power Sources* **2021**, *490*, 229504.

[11] J. Qian, B. D. Adams, J. Zheng, W. Xu, W. A. Henderson, J. Wang, M. E. Bowden, S. Xu, J. Hu, J.-G. Zhang, *Adv. Funct. Mater.* **2016**, *26*, 7094.

[12] Z. Xie, Z. Wu, X. An, X. Yue, J. Wang, A. Abudula, G. Guan, *Energy Storage Mater.* **2020**, *32*, 386.

[13] S. Nanda, A. Gupta, A. Manthiram, *Adv. Energy Mater.* **2021**, *11*, 2000804.

[14] D.-J. Yoo, K. J. Kim, J. W. Choi, *Adv. Energy Mater.* **2018**, *8*, 1702744.

[15] B. Wu, C. Chen, L. H. J. Raijmakers, J. Liu, D. L. Danilov, R.-A. Eichel, P. H. L. Notten, *Energy Storage Mater.* **2023**, *57*, 508.

[16] A. M. Haregewoin, A. S. Wotango, B.-J. Hwang, *Energy Environ. Sci.* **2016**, *9*, 1955.

[17] J. Zheng, M. H. Engelhard, D. Mei, S. Jiao, B. J. Polzin, J.-G. Zhang, W. Xu, *Nat. Energy* **2017**, *2*, 17012.

[18] D. Huang, C. Zeng, M. Liu, X. Chen, Y. Li, S. Hu, Q. Pan, F. Zheng, Q. Li, H. Wang, *Chem. Eng. J.* **2023**, *454*, 140395.

[19] H. Ye, Y. X. Yin, S. F. Zhang, Y. Shi, L. Liu, X. X. Zeng, R. Wen, Y. G. Guo, L. J. Wan, *Nano Energy* **2017**, *36*, 411.

[20] A. A. Assegie, C. C. Chung, M. C. Tsai, W. N. Su, C. W. Chen, B. J. Hwang, *Nanoscale* **2019**, *11*, 2710.

[21] S. Li, Z. Luo, L. Li, J. Hu, G. Zou, H. Hou, X. Ji, *Energy Storage Mater.* **2020**, *32*, 306.

[22] K. Lu, C. Chen, Y. Wu, C. Liu, J. Song, H. Jing, P. Zhao, B. Liu, M. Xia, Q. Hao, W. Lei, *Chem. Eng. J.* **2023**, *457*, 141287.

[23] Z. L. Brown, S. Jurng, B. L. Lucht, *J. Electrochem. Soc.* **2017**, *164*, A2186.

[24] Z. T. Wondimkun, T. T. Beyene, M. A. Weret, N. A. Sahalie, C.-J. Huang, B. Thirumalraj, B. A. Jote, D. Wang, W.-N. Su, C.-H. Wang, G. Brunklaus, M. Winter, B.-J. Hwang, *J. Power Sources* **2020**, *450*, 227589.

[25] Z. Yu, H. Wang, X. Kong, W. Huang, Y. Tsao, D. G. Mackanic, K. Wang, X. Wang, W. Huang, S. Choudhury, Y. Zheng, C. V. Amanchukwu, S. T. Hung, Y. Ma, E. G. Lomeli, J. Qin, Y. Cui, Z. Bao, *Nat. Energy* **2020**, *5*, 526.

[26] T. Li, X.-Q. Zhang, P. Shi, Q. Zhang, *Joule* **2019**, *3*, 2647.

[27] T. M. Hagos, G. B. Berhe, T. T. Hagos, H. K. Bezabh, L. H. Abrha, T. T. Beyene, C.-J. Huang, Y.-W. Yang, W.-N. Su, H. Dai, B.-J. Hwang, *Electrochim. Acta* **2019**, *316*, 52.

[28] B. T. Hotasi, T. M. Hagos, C. J. Huang, S.-K. Jiang, B. A. Jote, K. N. Shitaw, H. K. Bezabh, C.-H. Wang, W.-N. Su, S.-H. Wu, B. J. Hwang, *J. Power Sources* **2022**, *548*, 232047.

[29] J. Zhang, H. Zhang, L. Deng, Y. Yang, L. Tan, X. Niu, Y. Chen, L. Zeng, X. Fan, Y. Zhu, *Energy Storage Mater.* **2023**, *54*, 450.

[30] T. T. Hagos, B. Thirumalraj, C. J. Huang, L. H. Abrha, T. M. Hagos, G. B. Berhe, H. K. Bezabh, J. Cherng, S. F. Chiu, W. N. Su, B. J. Hwang, *ACS Appl. Mater. Interfaces* **2019**, *11*, 9955.

[31] A. Pei, G. Zheng, F. Shi, Y. Li, Y. Cui, *Nano Lett.* **2017**, *17*, 1132.

[32] K. Yan, Z. Lu, H.-W. Lee, F. Xiong, P.-C. Hsu, Y. Li, J. Zhao, S. Chu, Y. Cui, *Nat. Energy* **2016**, *1*, 16010.

[33] J.-J. Woo, V. A. Maroni, G. Liu, J. T. Vaughey, D. J. Gosztola, K. Amine, Z. Zhang, *J. Electrochem. Soc.* **2014**, *161*, A827.

[34] A. von Wald Cresce, O. Borodin, K. Xu, *J. Phys. Chem. C* **2012**, *116*, 26111.

[35] X.-B. Cheng, R. Zhang, C.-Z. Zhao, F. Wei, J.-G. Zhang, Q. Zhang, *Adv. Sci.* **2016**, *3*, 1500213.

[36] F. Han, Z. Chang, X. Liu, A. Li, J. Wang, H. Ding, S. Lu, *J. Phys. Conf. Ser.* **2021**, *2009*, 012069.

[37] X. Ren, Y. Zhang, M. H. Engelhard, Q. Li, J.-G. Zhang, W. Xu, *ACS Energy Lett.* **2017**, *3*, 14.

[38] H. Xiang, P. Shi, P. Bhattacharya, X. Chen, D. Mei, M. E. Bowden, J. Zheng, J.-G. Zhang, W. Xu, *J. Power Sources* **2016**, *318*, 170.

[39] R. Schmitz, R. Müller, S. Krüger, R. W. Schmitz, S. Nowak, S. Passerini, M. Winter, C. Schreiner, *J. Power Sources* **2012**, *217*, 98.

[40] R. Schmitz, R. Ansgar Müller, R. Wilhelm Schmitz, C. Schreiner, M. Kunze, A. Lex-Balducci, S. Passerini, M. Winter, *J. Power Sources* **2013**, *233*, 110.

[41] N. Koura, S. Kohara, K. Takeuchi, S. Takahashi, L. A. Curtiss, M. Grimsditch, M.-L. Saboungi, *J. Mol. Struct.* **1996**, *382*, 163.

[42] P. Verma, P. Maire, P. Novák, *Electrochim. Acta* **2010**, *55*, 6332.

[43] C. Chen, T. Zhou, D. L. Danilov, L. Gao, S. Benning, N. Schön, S. Tardif, H. Simons, F. Hausen, T. U. Schülli, R. A. Eichel, P. H. L. Notten, *Nat. Commun.* **2020**, *11*, 3283.

[44] K. Schroder, J. Alvarado, T. A. Yersak, J. Li, N. Dudney, L. J. Webb, Y. S. Meng, K. J. Stevenson, *Chem. Mater.* **2015**, *27*, 5531.

[45] R. E. Ruther, A. F. Callender, H. Zhou, S. K. Martha, J. Nanda, *J. Electrochem. Soc.* **2014**, *162*, A98.

[46] X. Zhang, A. Mauger, Q. Lu, H. Groult, L. Perrigaud, F. Gendron, C. M. Julien, *Electrochim. Acta* **2010**, *55*, 6440.

[47] C. Sole, N. E. Drewett, L. J. Hardwick, *Faraday Discuss.* **2014**, *172*, 223.

[48] S. Jiao, J. Zheng, Q. Li, X. Li, M. H. Engelhard, R. Cao, J.-G. Zhang, W. Xu, *Joule* **2018**, *2*, 110.

[49] A. J. Louli, M. Coon, M. Genovese, J. deGooyer, A. Eldesoky, J. R. Dahn, *J. Electrochem. Soc.* **2021**, *168*, 020515.

[50] P. Dan, E. Mengeritsky, D. Aurbach, I. Weissman, E. Zinigrad, *J. Power Sources* **1997**, *68*, 443.

[51] S. Jovanovic, P. Jakes, S. Merz, R. A. Eichel, J. Granwehr, *Electrochem. Sci. Adv.* **2022**, *2*, e2100068.